

The Wandering Supermassive Black Hole Powering the off-nuclear TDE AT2024tvd

M. GUOLO ,¹ A. MUMMERY,² S. VAN VELZEN ,³ M. NICHOLL ,⁴ S. GEZARI ,⁵ Y. YAO ,^{6,7} K. C. CHAMBERS ,⁸ T. DE BOER ,⁸ M. E. HUBER ,⁸ C.-C. LIN ,⁸ T. B. LOWE ,⁸ E. A. MAGNIER ,⁸ G. PAEK ,⁸ AND R. WAINSCOAT ,⁸

¹ Bloomberg Center for Physics and Astronomy, Johns Hopkins University, 3400 N. Charles St., Baltimore, MD 21218, USA

² School of Natural Sciences, Institute for Advanced Study, 1 Einstein Drive, Princeton, NJ 08540, USA

³ Leiden Observatory, Leiden University, Postbus 9513, 2300 RA Leiden, NL

⁴ Astrophysics Research Centre, School of Mathematics and Physics, Queen's University Belfast, Belfast BT7 1NN, UK

⁵ Department of Astronomy, University of Maryland, College Park, MD, 20742-2421, USA

⁶ Miller Institute for Basic Research in Science, 206B Stanley Hall, Berkeley, CA 94720, USA

⁷ Department of Astronomy, University of California, Berkeley, CA 94720-3411, USA

⁸ Institute for Astronomy, University of Hawaii, 2680 Woodlawn Dr., Honolulu, HI 96822, USA

ABSTRACT

We present an analysis of the spectral energy distribution (SED) of the off-nuclear tidal disruption event (TDE) AT2024tvd during its late-time plateau phase, combining X-ray spectra and UV/optical photometry. Using a fully relativistic, compact accretion disk model with self-consistent inner-disk Comptonization, we reproduce the observed SED without significant residuals. The inferred black hole mass $\log_{10}(M_\bullet/M_\odot) \approx 6.0 \pm 0.2$, and the inferred disk parameters place AT2024tvd within known TDE-disk scaling relations ($L_{\text{bol}}/L_{\text{Edd}} \propto T_p^4 \propto M_\bullet^{-1}$, $L_{\text{plat}} \propto M_\bullet^{2/3}$, $R_{\text{out}}/r_g \propto M_\bullet^{-2/3}$). Our results show that: (i) there is no *detected* star cluster or dwarf galaxy associated with the source, down to a mass limit of $\log_{10}(M_{\text{gal}}/M_\odot) \leq 7.6$; (ii) the black hole is a wandering supermassive, rather than intermediate-mass, black hole; and (iii) the source represents an extreme case of black hole-to-host mass ratio, with $M_\bullet/M_{\text{gal}} > 3\%$, consistent with a heavily tidally stripped nucleus. The latter aligns with cosmological simulations predicting that surviving host remnants of most wandering black holes should not retain a detectable stellar overdensity when located at small halo-centric distances. We discuss differences with previous analyses of this source and highlight why our modeling approach provides a more physically consistent solution with more reliable parameter inference.

Keywords: Accretion (14); High energy astrophysics (739); Supermassive black holes (1663); X-ray transient sources (1852); Time domain astronomy (2109)

1. INTRODUCTION

The scattering of a star within the radius of influence of a black hole onto a radial orbit that crosses its tidal radius can produce a luminous tidal disruption event (TDE; Rees 1988; Gezari et al. 2021). Such events are among the few observational probes of the existence and properties of otherwise quiescent BHs at distances beyond those of the nearest galaxies, where dynamical modeling of stars and gas is still feasible. We have now entered the era of population-level studies of TDEs, with more than 100 candidates and dozens of extremely well-observed sources whose basic multi-wavelength emission properties have been mapped out (e.g., van Velzen et al. 2021; Charalampopoulos et al. 2022; Yao et al. 2023; Guolo et al. 2024; Cendes et al. 2024; Mummery et al.

2024b; Grotova et al. 2025; Mummery & van Velzen 2025).

Inferring the properties of a black hole, particularly its mass (M_\bullet), directly from the emission produced by a TDE has proven challenging. Physical models developed to explain the poorly understood early-time optical flare have systematically failed (see Hammerstein et al. 2022; Ramsden et al. 2022; Guolo et al. 2025b) to recover, at a statistically significant level, known correlations between the derived M_\bullet values and host galaxy properties (Gültekin et al. 2009; Kormendy & Ho 2013; Reines & Volonteri 2015; Greene et al. 2020), including total stellar mass (M_{gal}), bulge mass (M_{bulge}), and velocity dispersion (σ_*).

In contrast, methods based on the late-time UV/optical plateau (Mummery et al. 2024b) and/or the X-ray emission (Guolo & Mummery 2025; Guolo et al. 2025b), both known to be powered by direct emission from the newly formed (expanding) accretion disk (Cannizzo et al. 1990; Mummery & Balbus 2020), have been shown to independently reproduce, with high statistical significance, all three correlations: M_{\bullet} – M_{gal} , M_{\bullet} – M_{bulge} , and M_{\bullet} – σ_* (Mummery et al. 2024b; Ramsden et al. 2025; Guolo et al. 2025b).

Such methods, which can derive M_{\bullet} values directly from the observed emission itself—without *assuming* any host-scaling relation but instead aiming to probe and populate such correlations—are essential as we begin to unveil a population of TDEs in environments where these scaling relations are not applicable.

The discovery of 3XMM J2150–05 (Lin et al. 2018, 2020) marks the first off-nuclear TDE; the source is associated with an ultra-compact dwarf (UCD) galaxy with $\log_{10}(M_{\text{gal}}/M_{\odot}) = 7.3 \pm 0.3$, located in the outskirts of a much more massive early-type galaxy ($M_{\star} \sim 10^{11} M_{\odot}$). Another such UCD/off-nuclear TDE, EP240222a, with very similar characteristics, was discovered by the Einstein Probe mission (Yuan et al. 2018) and reported by Jin et al. (2025). Disk modeling of both sources yields black hole masses in the intermediate-mass black hole (IMBH; $10^4 < M_{\bullet}/M_{\odot} \lesssim 10^5$) regime (Jin et al. 2025; Guolo et al. 2025b).

More recently, the first off-nuclear TDE discovered by an optical survey, AT2024tvd (Yao et al. 2025), shows all the classical characteristics of a TDE but is located 0.8 kpc (projected distance) from the nucleus of another massive ($M_{\star} \sim 10^{11} M_{\odot}$) early-type galaxy. Distinct from the previous two sources, pre-TDE images at the position of AT2024tvd reveal no clear stellar counterpart other than the halo of the parent galaxy, and modeling and subtraction of the parent galaxy surface brightness profile show no residuals down to an limit of $\log_{10}(M_{\text{gal}}/M_{\odot}) \leq 7.6$ (Yao et al. 2025).

The growing number of such sources appears to be opening a new window into the discovery of a population of off-nuclear IMBHs and/or wandering supermassive black holes (SMBHs), long predicted theoretically to exist (Volonteri et al. 2008; Ricarte & Natarajan 2018; Inayoshi et al. 2020; Ricarte et al. 2021b). These are however difficult to detect, as gas accretion onto these systems should be negligibly low in the local universe (Ricarte et al. 2021a,b). Non-accreting WBHs have been inferred dynamically in a small number of ultra-compact dwarf galaxies (UCDs; e.g., Seth et al. 2014; Taylor et al. 2025), which are common in galaxy clusters (Pfeffer et al. 2014; Voggel et al. 2019). Therefore

the transient, high accretion rate reached following a TDE possibly the most effective way to unambiguously discover and characterize the accreting counter-parts of these WBH systems.

The goals of this paper are to present follow-up observations of AT2024tvd, capturing the transition of its UV/optical light curve to the plateau phase, as well as novel high signal-to-noise ratio *XMM-Newton* X-ray spectra. This comprehensive multi-wavelength data facilitate full spectral energy distribution (SED) fitting to measure AT2024tvd’s black hole mass M_{\bullet} . This method has been shown to yield precise, reliable, and self-consistent results, including the ability to reproduce host-scaling relations with high statistical significance (Guolo et al. 2025b).

This paper is organized as follows. In §2, we present the data and fitting method; in §3, we describe the results of our SED fitting; in §4, we discuss these results, including their relation to previous work on the source; and in §5, we provide our conclusions. A Bayesian statistics framework is used throughout the paper, converging posterior of the inferred parameters are reported as median and the uncertainties correspond to the 68% credible intervals, unless otherwise stated.

2. DATA AND FITTING

The data used in this work are primarily public, including light curves from the Zwicky Transient Facility (ZTF; Bellm et al. 2019), observations from the Ultraviolet/Optical Telescope (UVOT; Roming et al. 2005) and the X-Ray Telescope (XRT; Burrows et al. 2005) on board the *Neil Gehrels Swift Observatory* (Gehrels et al. 2004), and diffraction-limited UV/optical/IR imaging from the *Hubble Space Telescope* (HST) and the *James Webb Space Telescope* (JWST), which are used to produce the RGB composite shown in Figure 1. We also present novel proprietary high signal-to-noise ratio X-ray spectra from *XMM-Newton* (OBSID 0942540601-901; PI: Guolo) obtained at two epochs, as well as deep late-time ground-based photometry from Pan-STARRS (Chambers et al. 2016). Details of the data reduction, including host-light subtraction, are provided in Appendix A.

In the right panel of Fig. 1, we show the multi-wavelength light curve of AT2024tvd. Two key properties of the source are now evident from the extended follow-up beyond the data presented in the discovery paper. First, the transient appears to have reached its plateau phase (Mummery et al. 2024b) around 250 days after discovery ($\Delta t \sim 250$ days). This is seen most clearly in the UV light curve, which decayed by a factor of ~ 10 during the first 100 days after peak (MJD

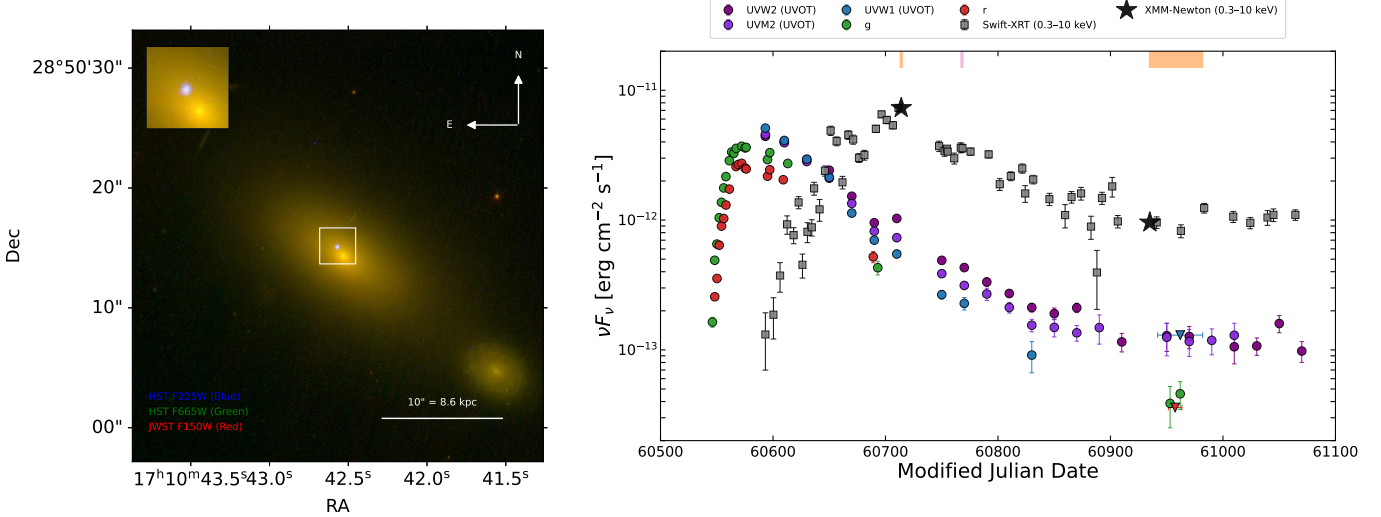


Figure 1. Left: diffraction limit RGB image of AT2024tvd using HST+JWST imaging. Right: multi-wavelength light curves of AT2024tvd, with the orange marker showing the epochs in which our SED fitting was performed. For plotting purposes the UVOT light curves were binned to have no more than one point each five days.

60600–60700), by an additional factor of $\lesssim 10$ over the following 100 days (MJD 60700–60800), and then remained statistically consistent with being constant over the next 150 days (MJD 60850–61100).

Second, the X-ray peak is now clearly identified as having occurred around $\Delta t \sim 150$ days, or approximately 100 days after the optical/UV peak—behavior that is not uncommon among TDEs (Guolo et al. 2024). Our first *XMM-Newton* epoch appears to coincide closely with this X-ray peak. By the time of the second *XMM-Newton* epoch, the source had entered the plateau phase in its UV/optical light curve. At this epoch, ZTF no longer detected the transient, but our deep Pan-STARRS follow-up securely detected the source in the *g*-band and placed deep upper limits in the *r*-band. The Pan-STARRS observations are quasi-simultaneous with the second *XMM-Newton* epoch, taken approximately 10 days apart.

To derive the physical properties of AT2024tvd, we perform full SED fitting. Following Guolo et al. (2025b), we use the color-corrected relativistic compact disk model `kerrSED` (Guolo & Mummery 2025) to fit one epoch of X-ray spectra plus UV/optical photometry during the plateau phase, as well as another epoch of X-ray spectra *only*, corresponding to the time when the X-rays were near peak flux. The rationale behind these choices is discussed in detail by Guolo et al. (2025b), but can be summarized based on several key aspects of TDEs. First, the UV/optical plateau is produced by direct emission from the outer regions of a compact, expanding disk (Mummery et al. 2024b). Second, the same disk powers the X-ray emission at all times (as shown independently through individual source fitting

and luminosity function analysis; see Mummery & Balbus 2020; Mummery & van Velzen 2025; Guolo et al. 2025b). Third, the early-time optical emission (prior to the plateau) is *not* produced by direct disk emission, and cannot be modeled with such models. These facts imply that during the plateau phase, the entire SED is generated by direct disk emission and can therefore be reliably modeled with such models, but that is not true prior to the plateau. Nevertheless, the peak X-ray epoch, being sourced by the same disk, still aides in constraining black hole properties, particularly helping to break degeneracies between dynamical and intrinsic parameters (see discussion in Guolo et al. 2025b).

For the X-rays, we use two *XMM-Newton* spectra that satisfy the above conditions. For the second epoch (full SED), we include both UVOT and Pan-STARRS data (including both detections and upper limits). These two epochs are marked in orange in Figure 1. The fitting is carried out using the Bayesian X-ray Analysis software (BXA) version 4.0.7 (Buchner et al. 2014), which connects the nested sampling algorithm `UltraNest` (Buchner 2019) with the `PyXspec` fitting environment (Arnaud 1996a). The two epochs are loaded and fitted simultaneously under the assumption of Gaussian statistics.

In addition to the disk model, we account for both Galactic – using `phabs×redder` and assuming known values for column density and color excess (HI4PI Collaboration et al. 2016; Schlafly & Finkbeiner 2011) – and intrinsic (using `phabs×redderSF`) absorption and reddening due to gas and dust along the line of sight. The source emission is redshifted to the measured redshift z using `zashift`. In `XSPEC` notation, the model is `phabs×redder×zashift (phabs×redderSF×(SimPL×`

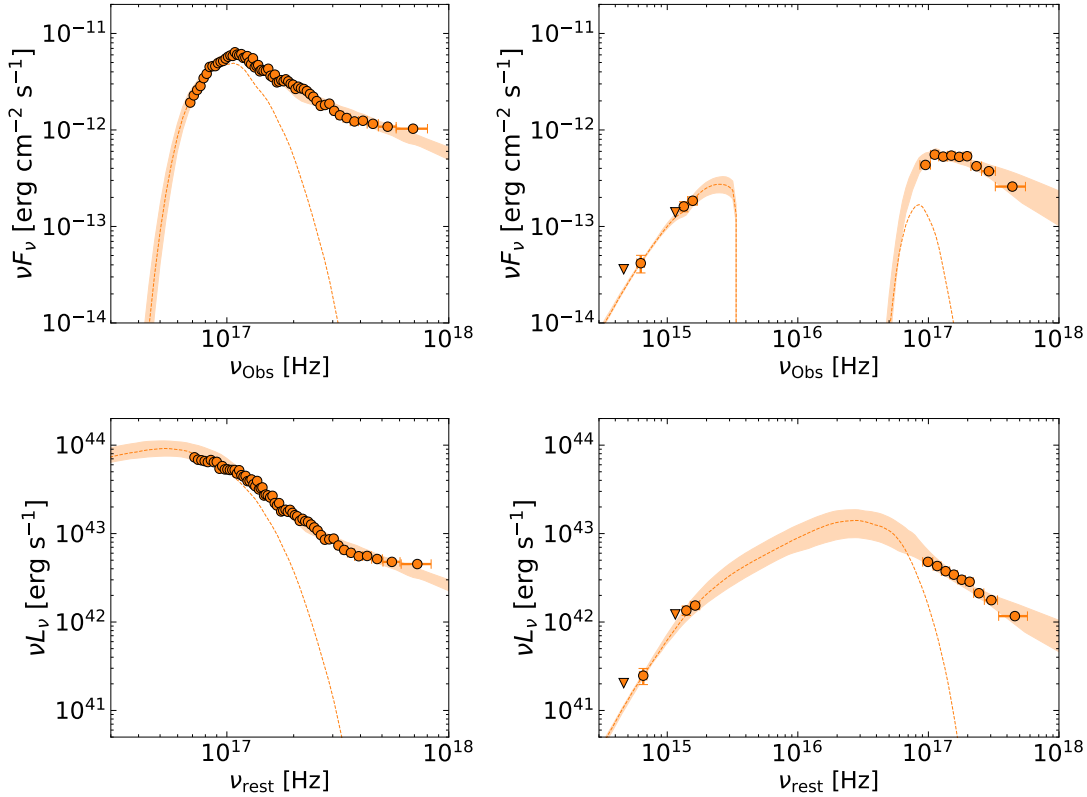


Figure 2. Spectral energy distribution modeling of AT2024tvd. The upper panels show the emission in the observer frame, while the lower panels display the rest-frame emission corrected for all absorption and extinction/attenuation effects. The left column presents the early-time, disk-dominated *XMM-Newton* spectrum, which is well reproduced within an inner accretion disk plus corona framework. At later times, the full optical/UV–X-ray SED is consistently reproduced using the same disk framework (right column). The dashed lines indicate the median disk solutions with the coronal component turned off.

`kerrSED`), where `SimPL` (Steiner et al. 2009) is used to self-consistently account for strong Comptonization (i.e., the hard X-ray tail), while conserving the number of photons—an important feature of AT2024tvd’s X-ray spectra (Yao et al. 2025).

We adopt the same priors and parameter limits as described in Guolo et al. (2025b). In the fitting process, the five free parameters of `kerrSED`—inner disk radius (R_{in}), peak disk temperature (T_p), outer disk radius (R_{out}), black hole spin (a_{\bullet}), and inclination angle (i)—are treated as follows: T_p and R_{out} , being dynamical, are allowed to vary between epochs, while the remaining parameters are tied between the two epochs. However, since the first epoch includes X-ray data only (as the early-time optical flare is not powered by the disk), $R_{\text{out}}(E1)$ is completely unconstrainable, and is simple assumed to be $R_{\text{out}}(E1) \leq R_{\text{out}}(E2)$, a physical prior resulting from angular momentum conservation. The corona/`SimPL` parameters (f_{sc} and Γ) are treated as independent and free parameters. The posterior on black hole mass, and disk bolometric luminosity ($L_{\text{Bol}}^{\text{disk}}$) are then extracted from the posteriors of the free parameters, see equation 3 and 4 in Guolo et al. (2025b).

3. RESULTS

The resulting SED fitting is shown in Fig. 2. The left panel presents the first *XMM-Newton* epoch, obtained near the X-ray peak, where the spectrum is well described by a hot inner disk with a modest contribution from a Comptonising corona. The second epoch, corresponding to when the UV/optical emission has entered the plateau phase, is fully accounted for by emission from a compact disk whose inner regions are now dominated by stronger Comptonization.

Crucially, for the discussion in §4, the combined X-ray spectra and UV/optical SED can be modeled with no significant residuals in the second disk-dominated plateau phase epoch. This indicates that the disk (plus corona) emission alone can explain all of the observed, pre-transient-subtracted flux during the second epoch. The median values and 1σ uncertainties of the inferred parameters are summarized in Table 1, while the full posterior distributions are shown in Appendix B.

Table 1. Summary of Inferred Parameters

Δt (days)	$\log_{10}(N_{\text{H}})$ (cm $^{-2}$)	$E(B - V)^{(a)}$	$\log_{10}(R_{\text{in}})$ (km)	$\log_{10}(T_{\text{p}})$ (K)	$\log_{10}(R_{\text{out}})$ (r_g)	$\log_{10}(M_{\bullet})$ (M_{\odot})	$\log_{10}(L_{\text{Bol}}^{\text{disk}})$ (erg s $^{-1}$)	$\log_{10}(L_{\text{Bol}}^{\text{disk}}/L_{\text{Edd}})$
168	$20.60^{+0.20}_{-0.24}$	$0.04^{+0.03}_{-0.02}$	$6.93^{+0.08}_{-0.07}$	$5.70^{+0.04}_{-0.04}$	—	—	$44.27^{+0.08}_{-0.09}$	$0.17^{+0.09}_{-0.12}$
389-436				$5.49^{+0.05}_{-0.05}$	$2.80^{+0.13}_{-0.13}$	$6.00^{+0.19}_{-0.16}$	$43.45^{+0.17}_{-0.19}$	$-0.67^{+0.18}_{-0.16}$

NOTE— Δt refer to time since first detection of the source.

From the fitting, we obtain, importantly, $\log_{10}(R_{\text{in}}/\text{km}) \approx 6.9 \pm 0.1$, $|a_{\bullet}| \lesssim 0.5$ (90% credible interval) and $i \lesssim 60$ deg (90% credible interval), from these we infer a black hole mass of $\log_{10}(M_{\bullet}/M_{\odot}) = 6.00^{+0.19}_{-0.14}$. This result is illustrated in Fig. 3, where AT2024tvd is placed within the accretion disk parameter space of other TDEs systems (alongside 14 other events modeled with the same relativistic disk framework, `kerrSED`).¹

In Fig. 3, the left panels show standard accretion disk correlations, $L_{\text{bol}}^{\text{disk}}/L_{\text{Edd}} \propto T_{\text{p}}^4 \propto M_{\bullet}^{-1}$, while the right panels display TDE-specific correlations, $L_{\text{plat}} \propto M_{\bullet}^{2/3}$ and $R_{\text{out}}/r_g \propto M_{\bullet}^{-2/3}$. In the upper-right panel, the earliest measurements of R_{out}/r_g for each source are shown, color-coded by time since discovery. The solid black line marks the circularization radius, $R_{\text{circ}} \propto M_{\bullet}^{-2/3}$, normalized for the disruption of a solar-mass main-sequence star with an impact parameter $\beta = 1$. The lower-right panel presents the plateau luminosity, L_{plat} , computed from the modeled νL_{ν} SED at $\nu = 10^{15}$ Hz and evaluated at the closest epoch to $\Delta t = 1000$ days, overlaid on the 10^6 time-dependent disk solutions from Mummery et al. (2024b) at the same epoch and frequency (i.e., their $L_{\text{plat}} - M_{\bullet}$ scaling relation, all of these theoretical points are evaluated at 1000 days).

From its spectral and multi-wavelength properties, AT2024tvd is therefore indistinguishable from classical, nuclear TDEs powered by SMBHs, confirming that its emission originates from a supermassive, rather than intermediate-mass, black hole.

All correlations in Fig. 3 follow naturally from classical time-dependent disk theory (Lynden-Bell & Pringle 1974; Cannizzo et al. 1990; Balbus 2017; Mummery & Balbus 2020). In particular, the relations shown in the right panels emerge when this framework is ap-

plied to disks forming near R_{circ} that subsequently expand to conserve angular momentum (see, e.g., Mummery et al. 2024b,a; Guolo et al. 2025a). In this parameter space, every TDE with $\log_{10}(M_{\bullet}/M_{\odot}) > 5$ (except AT2024tvd) is a nuclear or “normal” TDE, while the outlier at $\log_{10}(M_{\bullet}/M_{\odot}) \approx 4.4$ corresponds to the off-nuclear IMBH TDE 3XMM J2150–05, associated with a detected ultra-compact dwarf galaxy (UCD, $M_{\text{gal}} \sim 10^7 M_{\odot}$).

4. DISCUSSION

4.1. Comparison to previous studies

It is important to compare the results obtained in the previous section with those reported in the two previous analyses of AT2024tvd. The discovery paper by Yao et al. (2025) presented data covering only the early decline of the optical flare and was limited to observations obtained prior to the X-ray peak. In that study, the authors estimated the black hole mass using two different methods.

First, the authors fitted the optical/UV light curve using `MOSFIT` (Mockler et al. 2019). While the resulting black hole mass estimate is statistically consistent with the value derived in this work, this agreement is not surprising. `MOSFIT` is known to systematically recover black hole masses clustered around $\log_{10}(M_{\bullet}/M_{\odot}) \sim 6.5 \pm 0.5$ (1σ), largely independent of host galaxy properties (e.g., left panel Fig. 12 of Guolo et al. 2025b) such that it is unable to recover any of the known black hole–host galaxy scaling relations (Hammerstein et al. 2023; Ramsden et al. 2022; Guolo et al. 2025b). This is likely because its assumed luminosity scaling (with the fallback rate) is in strong conflict with the TDE population data (Mummery et al. 2025), implying that the derived masses are not reliable.

Second, the authors employed the *empirical* correlation between the peak optical luminosity of nuclear TDEs and black hole mass derived by Mummery et al. (2024b), obtaining $\log_{10}(M_{\bullet}/M_{\odot}) = 6.9 \pm 0.5$. While this relation is, by construction, consistent with the data on a population level, and provides a useful first-order

¹ Importantly, the masses derived from this model reproduce the classical M_{\bullet} – M_{gal} and M_{\bullet} – σ_{\star} relations with high statistical significance (Guolo et al. 2025b), unlike masses derived from modeling of TDE optical flares (see §1 and references therein).

estimate (Mummetry 2026), it suffers from substantial intrinsic scatter, and is after all a scaling relation not modeling of the source emission itself. Moreover, there is currently no physical model capable of explaining this correlation in its entirety (see the detailed discussion in Mummetry et al. 2025).

More recently, the study by Patra et al. (2025, hereafter P25) attempted to infer several properties of AT2024tvd, including M_{\bullet} , from its multi-wavelength emission using an X-ray-to-IR analysis. While their approach may appear, at a surface level, similar to that adopted here, the two methods differ in several important aspects. These differences naturally account for the discrepancies between many of the values reported by P25 and those derived in this work.

In that work, the authors fit the SED of AT2024tvd at $\Delta t \sim 200$ days (marked as a pink tick in Fig. 1). Their data set consists of a JWST near-infrared spectrum, photometry in two UV bands from *Swift*/UVOT, r - and g -band photometry from ZTF, and the *integrated* 0.3–10 keV luminosity from *Swift*/XRT, represented as a single data point at ~ 20 Å (~ 0.6 keV). The optical photometry is based on difference imaging, while the UVOT fluxes have had pre-transient light subtracted using a stellar model derived from pre-transient imaging (from *GALEX* in the UV) within a 5'' aperture.

The resulting SED is modeled using a steady-state, non-GR-corrected accretion disk model (Shakura & Sunyaev 1973) with three free parameters (\dot{M}_{\bullet} , M_{\bullet} , and R_{out}/r_g), together with an additional cold blackbody component intended to represent dust-reprocessed emission at longer wavelengths. This model is unable to reproduce the full SED, leaving substantial residuals in the UV bands, which are then modeled with an additional stellar component interpreted as a stellar cluster associated with AT2024tvd. However, this inferred stellar component is based solely on UV residuals and is not supported by any direct detection of stellar emission in the JWST or other infrared data.

The claimed stellar counterpart is therefore inferred from residuals obtained after fitting a disk model at a time when the system had not yet reached the plateau phase. It is well established that the early-time UV/optical emission in TDEs is not produced by direct disk radiation (e.g., Gezari et al. 2009; van Velzen et al. 2011; Roth et al. 2020; Mummetry et al. 2025); consequently, fitting this phase with a disk model inevitably produces residuals at UV/optical wavelengths (e.g., Figure 15 in Guolo et al. 2024). Only during the plateau phase—once the early-time flare has completely faded—can the full SED be consistently modeled with a disk component (Mummetry & Balbus 2020;

Guolo et al. 2025b). The shallow infrared slope seen in the JWST data is likely due to non-thermal free-free emission, as seen in early-time emission of other TDEs (Reynolds et al. 2025). Trying to describe this (likely) reprocessed emission with a single disk will greatly overestimate the outer disk radius, which explains the (unphysically) large outer disk radius reported by P25.

Furthermore, the optical/UV modeling of P25 is performed on data from which pre-transient host light has already been subtracted. As a result, any genuine stellar emission at the TDE location will already have been removed. To put this simply, a stellar host (and any associated emission) cannot be recovered from host-subtracted photometry. We must therefore conclude that the nuclear star cluster claimed by P25 is an artifact of fitting an incorrect model to the early-time TDE emission. The upper limits on stellar light at the TDE location derived by Yao et al. (2025) remain valid and will be assumed in the following section.

Besides the claim for a NSC, the disk model of P25 is also used to estimate the mass of the black hole. In addition to the issues with the UV data analysis pointed out above, we also identify several problems with the treatment of the X-ray emission.

First of all, the X-ray emission is treated as a single luminosity measurement (at 0.6 keV), despite the fact that the observed 0.3–10 keV spectrum lies on the exponentially falling (quasi-Wien) tail of the emission. In this regime, the integrated luminosity alone cannot simultaneously constrain both \dot{M}_{\bullet} and M_{\bullet} , as their effects are strongly degenerate without spectral shape information². In practice, the inferred parameters depend sensitively on the arbitrary placement of the (single) X-ray data point within the full SED fitting, the approach by P25 is effectively discarding all the information (other than the integrated luminosity) contained in the X-ray spectra of the source.

Second, the X-ray spectra of AT2024tvd are not expected to be well described by pure thermal disk emission. Non-thermal Comptonized emission contributes significantly even at early times and dominates at later epochs (Fig. 2). Accurate mass inference therefore requires a self-consistent model that conserves photon number, accounting for disk photons that are up-scattered by the corona. In addition, the model employed by P25 does not include color-correction effects, which are required for meaningful disk-based measure-

² Unless multiple epochs are fitted simultaneously, allowing the effects of the dynamical (e.g., \dot{M}_{\bullet}) and intrinsic (M_{\bullet}) parameters to be disentangled, as in time-dependent approaches such as `FitTeD` (Mummetry et al. 2024a).

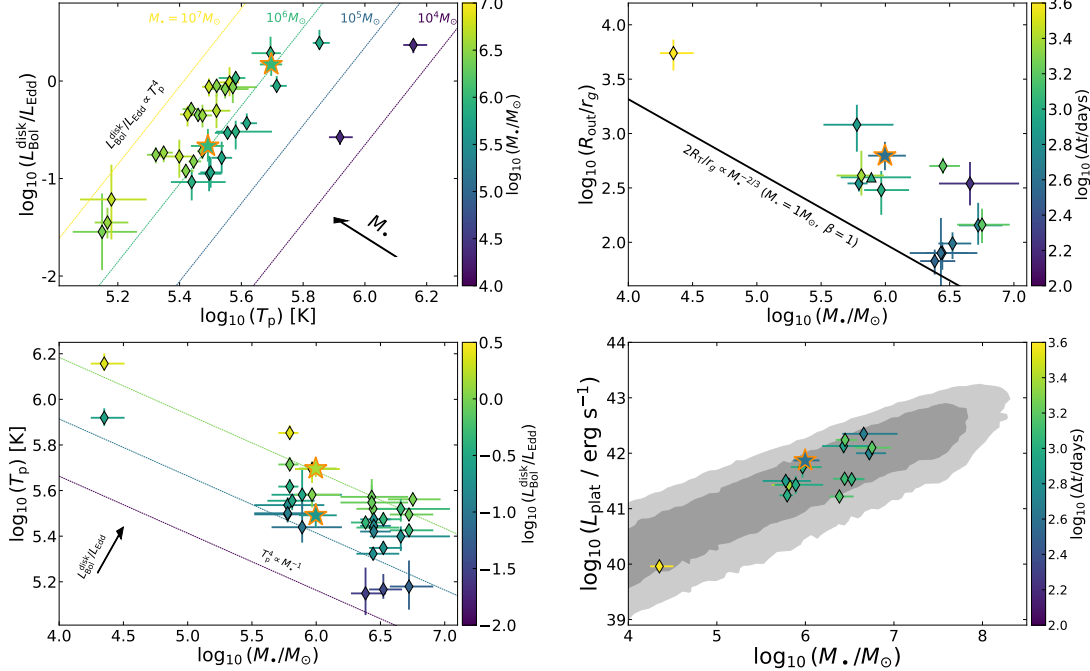


Figure 3. The location of AT2024tvd (points displayed by stars with orange outline) in the phase space spanned by TDE accretion disks (all other points; presented in Guolo et al. 2025b and derived with the same method and model). AT2024tvd has an accretion flow which is entirely consistent with the nuclear TDE population, i.e. powered by a SMBH. Left panels show standard accretions correlations between Eddington ratio, peak disk temperature and black hole mass. In these panels the lines of constant M_\bullet ($= 10^4, 10^5, 10^6$ and $10^7 M_\odot$) and constant $L_{\text{disk}}^{\text{disk}}/L_{\text{Edd}}$ ($= 0.01, 0.1, 1.0$) are computed for the case of $a_\bullet = 0$ and $R_{\text{out}} = 100r_g$. The right panels show correlation which are specific to TDE disks: between the UV luminosity of the plateau and the black hole mass (Mummery et al. 2024b), and between the relative size of the disk and the black hole mass. Every scaling relationship can be understood with respect to time-dependent disk theory (see text).

ments (Shimura & Takahara 1995; Hubeny et al. 2001; Davis & Hubeny 2006; Davis & El-Abd 2019; Mummery 2021). Neglecting both these effects leads to an underestimate of the intrinsic X-ray flux and, consequently, of the normalization parameter (i.e., M_\bullet in P25’s model). These factors explain the substantially lower mass of $M_\bullet \approx 3 \times 10^5 M_\odot$ inferred in that study. The combined underestimation of the black hole mass, and the attribution of early time non-disk emission, to disk emission, also explain the much higher (Eddington normalized) accretion ratio recovered by the authors. We have shown that AT2024tvd remains close to $L_{\text{Bol}}/L_{\text{Edd}} \sim 1$ even at peak X-ray luminosity (in common with many TDEs at peak, Mummery et al. 2023; Guolo et al. 2025b).

Given all of the above, we conclude that the parameters derived by P25—including M_\bullet , M_\bullet , R_{out} , as well as the claimed underlying nuclear star cluster—do not provide reliable measurements of the physical properties of AT2024tvd.

4.2. Implications for the Origin of AT2024tvd and for Black Hole Demographics

The inferred mass of the black hole powering AT2024tvd, $\log_{10}(M_\bullet/M_\odot) \approx 6.0 \pm 0.2$, provides strong

constraints on both the origin of the system and its implications for the broader population of black holes in the local Universe. This measurement places the source firmly within the supermassive regime, distinguishing it from the two previously known off-nuclear TDEs, 3XMM J2150–05 and EP240222a, which were consistent with IMBHs. AT2024tvd therefore demonstrates that not all off-nuclear TDEs arise from IMBHs still embedded in dwarf satellites in the outskirts of massive galaxies; instead, some originate from displaced, or wandering, SMBHs that have already sunk deep into the potential wells of their halos.

Although we discussed in the previous section how the properties inferred for both the black hole and its stellar counterpart by P25 are inconsistent with our findings, we nevertheless agree with their conclusion that the origin of the black hole is most consistent with a minor merger, rather than with gravitational recoil or dynamical ejection from the parent galactic nucleus. This conclusion follows from a simple statistical argument rooted in hierarchical galaxy formation, in which the number of minor mergers is far greater than the number of major mergers (e.g., Governato et al. 1994; Volonteri & Perna 2005). Moreover, the rate of minor mergers is expected

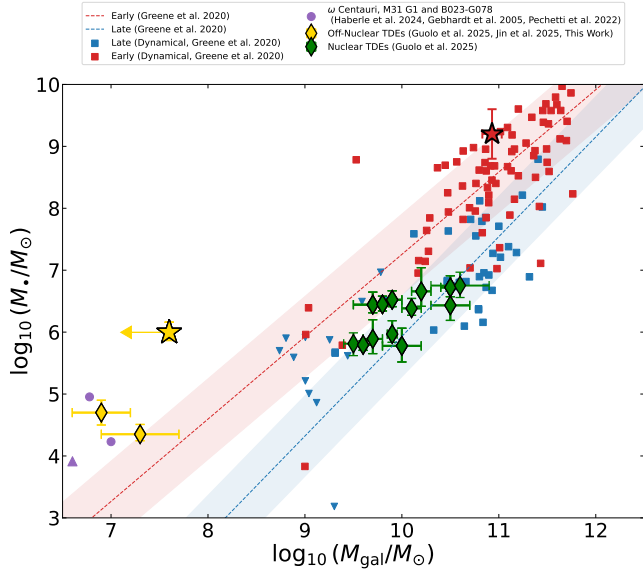


Figure 4. Black hole mass of AT2024tvd (yellow star) in the context of the host–black hole mass relation. Red and blue squares show dynamical black hole mass measurements in nearby galaxies (from Kormendy & Ho 2013; Greene et al. 2020), with contours indicating the corresponding correlations derived by Greene et al. (2020). Purple points denote dynamically inferred black holes in globular clusters (from Haberle et al. 2024; Gebhardt et al. 2005; Pechetti et al. 2022). Nuclear TDEs are shown as green diamonds (from Guolo et al. 2025b), while off-nuclear IMBH TDEs in ultra-compact dwarfs are shown as yellow diamonds (3XMM J2150–05 and EP20240222a; Lin et al. 2018; Guolo et al. 2025b; Jin et al. 2025). AT2024tvd is a strong outlier, with only an upper limit on its host stellar mass, consistent with a wandering SMBH embedded in a tidally stripped nucleus. The red star marks the central SMBH of AT2024tvd’s parent galaxy (detected in radio by Yao et al. 2025) with its mass estimated using the $M_{\bullet} - \sigma_{*}$ relation.

to scale with halo mass, which may naturally explain why all three known off-nuclear TDEs have been detected in massive galaxies (Bellovary et al. 2010; Ricarte et al. 2021b,a). This interpretation is further supported by the long dynamical friction timescales associated with mergers, which are often comparable to or longer than a Hubble time (Dosopoulou & Antonini 2017; Dvorkin & Barausse 2017). As a result, massive black holes accreted onto massive halos are expected to stall on wide orbits; in the local Universe, most therefore remain offset from the galactic nucleus, with only a small fraction forming close SMBH pairs (Tremmel et al. 2015, 2018b).

The extremely high stellar mass of the parent galaxy of AT2024tvd, its large nuclear velocity dispersion ($\sigma_{*} \sim 300 \text{ km s}^{-1}$, P25), and the detection of radio emission from its nucleus (Yao et al. 2025) also exclude the possibility that the black hole powering AT2024tvd

is the central SMBH to its halo. Using the $M_{\bullet} - \sigma_{*}$ scaling relations of Kormendy & Ho (2013), the central black hole is instead expected to have a mass of $\log_{10}(M_{\bullet}/M_{\odot}) \approx 9.2 \pm 0.4$, well above the Hills mass (the black hole mass scale at which stars are swallowed whole rather than disrupted, Hills 1975).

The location of AT2024tvd—approximately 0.8 kpc (projected) from the nucleus of a massive early-type galaxy with $M_{*} \sim 10^{11} M_{\odot}$ —together with the absence of any detected stellar overdensity down to $\log_{10}(M_{\text{gal}}/M_{\odot}) \leq 7.6$, strongly suggests that the black hole resides in a stripped remnant nucleus. This is clearly illustrated in Fig. 4, which shows the $M_{\bullet} - M_{\text{gal}}$ plane comparing the dynamical black hole mass compilations of Kormendy & Ho (2013) and Greene et al. (2020) with masses inferred from nuclear TDEs (green symbols; Guolo et al. 2025b) and from the three off-nuclear TDEs (yellow symbols): EP20240222a, 3XMM J2150–05, and AT2024tvd, with masses taken from Jin et al. (2025), Guolo et al. (2025b), and this work, respectively. The black hole masses for all TDEs are derived using the same method and model, except for EP20240222a, which employs a slightly different approach but yields results broadly consistent with `kerrSED` (see discussion in Guolo et al. 2025b). In this figure, the stripped-nucleus nature of AT2024tvd is evident, as the source stands out with an unusually high black hole to stellar mass ratio, $M_{\bullet}/M_{\text{gal}} > 0.03$.

This interpretation is fully consistent with predictions from cosmological simulations such as ROMULUS (Tremmel et al. 2018a; Ricarte et al. 2021b), which show that hierarchical galaxy assembly naturally produces a population of wandering MBHs, that can be broadly—though not exclusively—divided into two classes: black holes that remain far from the halo center and retain some (if not most) of their stellar counterparts, residing in dwarf satellites (as in EP20240222a and 3XMM J2150–05) or even massive globular clusters, and a second population that has migrated deeper into the halo potential but has been stripped of most their associated (resolved) stellar population and show no detectable stellar over density. This of course does not mean that they have no associated stellar population, e.g., a dense nuclear cluster which can more easily avoid tidal stripping (Van Wassenhove et al. 2014; Tremmel et al. 2018b) but may be unresolved/undetectable at the available resolution, but can be massive/dense enough to produce TDEs at a detectable rate.

AT2024tvd appears to be the first observed example of this latter population. In a companion paper (Guolo, in prep.), we show that the properties of off-nuclear TDEs, their host galaxies, and their spatial distribution closely

match the predictions of these simulations, even with the currently small sample size.

This discovery has broader implications for black hole demographics. The ability to measure M_\bullet directly from the multi-wavelength emission of a TDE—using a physical model that can independently reproduce host scaling relations, but without assuming them—point towards off-nuclear TDE being likely the only independent way to place constraints on the mass distribution of wandering black holes. More generally, AT2024tvd empirically links the transient accretion population to the wandering black hole population predicted by cosmological simulations, bridging the gap between theoretical models of hierarchical growth and observable time-domain phenomena.

5. CONCLUSION

We have presented a detailed analysis of the full spectral energy distribution (SED) of the off-nuclear TDE AT2024tvd during its late-time plateau phase. Using a fully relativistic, compact accretion-disk model with self-consistent inner-disk Comptonization, we reproduce the observed emission without significant residuals. The inferred black hole mass, $\log_{10}(M_\bullet/M_\odot) \approx 6.0 \pm 0.2$, is robust and places AT2024tvd firmly in the SMBH regime, while remaining fully consistent with established disk-based scaling relations observed in TDEs ($L_{\text{bol}}^{\text{disk}}/L_{\text{Edd}} \propto T_p^4 \propto M_\bullet^{-1}$, $L_{\text{plat}} \propto M_\bullet^{2/3}$, $R_{\text{out}}/r_g \propto M_\bullet^{-2/3}$). We also revisited the properties inferred by previous studies and showed why the values derived here are more reliable and better grounded, both observationally and theoretically.

Our results demonstrate that the black hole powering AT2024tvd is fundamentally distinct from those associated with the two previously known off-nuclear TDEs, 3XMM J0251-05 and EP240222a, which were powered by IMBHs ($M_\bullet \lesssim 10^5 M_\odot$) and hosted in detected satellite ultra-compact dwarfs. The absence of any detectable stellar overdensity at the transient lo-

cation, combined with the extreme black hole-to-host mass ratio ($M_\bullet/M_{\text{gal}} > 3\%$), strongly supports an origin as a highly tidally stripped remnant nucleus hosting a wandering SMBH. This interpretation is consistent with expectations from hierarchical galaxy formation and with cosmological simulations (e.g., ROMULUS Ricarte et al. 2021b) predicting that most wandering black holes at small halo-centric distances should lack detectable surviving stellar counterparts.

More broadly, AT2024tvd demonstrates that off-nuclear TDEs can provide a direct and physically grounded probe of the wandering SMBH population in the local Universe. While upcoming wide-field optical surveys such as the Rubin Observatory Legacy Survey of Space and Time (LSST) are expected to discover many more off-nuclear TDEs, X-ray observations remain essential for achieving reliable and precise black hole mass measurements, as they directly trace emission from the innermost regions of the accretion disk. By enabling black hole mass estimates derived entirely from the transient emission and independent of host-galaxy scaling relations, off-nuclear TDEs offer a unique observational pathway to uncover and characterize displaced black holes that would otherwise remain undetectable.

Acknowledgments – MG is grateful to the Institute for Advanced Study for its hospitality, where part of this work was carried out, and thanks Zachary Lane for help with the color image in Figure 1. MG acknowledges support from NASA through XMM-Newton grant 80NSSC24K1885. A.M. acknowledges support from the Ambrose Monell Foundation, the W.M. Keck Foundation and the John N. Bahcall Fellowship Fund at the Institute for Advanced Study. MN is supported by the European Research Council (ERC) under the European Union’s Horizon 2020 research and innovation programme (grant agreement No. 948381). Pan-STARRS is a project of the Institute for Astronomy of the University of Hawaii, and is supported by the NASA SSO Near Earth Observation Program under grants 80NSSC18K0971, NNX14AM74G, NNX12AR65G, NNX13AQ47G, NNX08AR22G, 80NSSC21K1572 and by the State of Hawaii.

APPENDIX

A. DATA REDUCTION

We performed point-spread-function (PSF) photometry on all publicly available ZTF data using the ZTF

forced-photometry service (Masci et al. 2019, 2023) in the g and r bands.

We observed AT2024tvd using the Panoramic Survey Telescope and Rapid Response System (Pan-STARRS;

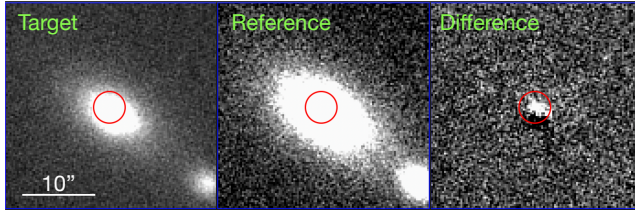


Figure 5. Late-time Pan-STARRS detection of AT2024tvd in g -band.

(Chambers et al. 2016) on 2025-10-05 and 2025-10-14, with 6×200 s exposures in the Pan-STARRS g_{P1} and r_{P1} filters on each night. All observations were processed and photometrically calibrated with the PS image processing pipeline (Magnier et al. 2020a,b; Waters et al. 2020), including subtraction of a deep reference image of the same field. The subtraction was complicated by the proximity of AT2024tvd to the bright galaxy nucleus (offset comparable to the full-width at half-maximum of the point-spread function). We downloaded and manually vetted all images, confirming a clear detection of flux in the g -band difference images at the position of AT2024tvd, which is shown in Fig. 5. We calculate the flux in each epoch as the mean flux from the reliable g -band subtractions. Negative residuals from the galaxy core prevented a clear detection in the r -band, and we report only an upper limit in this filter.

The *Swift*/UVOT photometry was analyzed using the `uvotsource` package with a $10''$ aperture. Host-galaxy flux was subtracted using estimates from population-synthesis modeling of archival pre-event photometry (Yao et al. 2025).

The 0.3–10 keV *Swift*/XRT light curves were generated using the UK Swift Data Centre online XRT data products tool (Evans et al. 2007), based on HEASOFT v6.22 (Arnaud 1996b), and binned by observation ID. For Fig. 1, count rates were converted to fluxes using the nearest best-fit X-ray spectral model from the two analyzed epochs (see main text).

Our primary data set consists of *XMM-Newton* observations obtained mainly through AO-23 program 94254 (P.I.: Guolo), targeting deep X-ray follow-up of ZTF-discovered TDEs. These data were taken in Full Frame mode with the thin filter using EPIC (Strüder et al. 2001) and are presented here for the first time. The observation data files were reduced using the *XMM-Newton* Standard Analysis Software (SAS; Gabriel et al. 2004). The raw data were processed with `epproc`, and only pn data were analyzed due to its superior sensitivity. Background flares were identified by inspecting 10–12 keV light curves and used to define good-time intervals. Events were filtered to include only single and double patterns (`PATTERN<=4`). Source and background spectra were extracted from circular regions of radii $r_{\text{src}} = 35''$ and $r_{\text{bkg}} = 108''$ on the same CCD. The ARFs and RMFs were generated using `arfgen` and `rmfgen`, respectively.

B. ADDITIONAL FIGURES

In Fig. 6 we show the full parameter posterior for the free parameters in our SED fitting, while in Fig. 7 we show the posterior on secondary derived parameters.

REFERENCES

Arnaud, K. A. 1996a, in Astronomical Society of the Pacific Conference Series, Vol. 101, Astronomical Data Analysis Software and Systems V, ed. G. H. Jacoby & J. Barnes, 17

Arnaud, K. A. 1996b, in Astronomical Society of the Pacific Conference Series, Vol. 101, Astronomical Data Analysis Software and Systems V, ed. G. H. Jacoby & J. Barnes, 17

Balbus, S. A. 2017, MNRAS, 471, 4832, doi: [10.1093/mnras/stx1955](https://doi.org/10.1093/mnras/stx1955)

Bellm, E. C., Kulkarni, S. R., Graham, M. J., et al. 2019, PASP, 131, 018002, doi: [10.1088/1538-3873/aaecbe](https://doi.org/10.1088/1538-3873/aaecbe)

Bellovary, J. M., Governato, F., Quinn, T. R., et al. 2010, ApJL, 721, L148, doi: [10.1088/2041-8205/721/2/L148](https://doi.org/10.1088/2041-8205/721/2/L148)

Buchner, J. 2019, PASP, 131, 108005, doi: [10.1088/1538-3873/aae7fc](https://doi.org/10.1088/1538-3873/aae7fc)

Buchner, J., Georgakakis, A., Nandra, K., et al. 2014, A&A, 564, A125, doi: [10.1051/0004-6361/201322971](https://doi.org/10.1051/0004-6361/201322971)

Burrows, D. N., Hill, J. E., Nousek, J. A., et al. 2005, SSRv, 120, 165, doi: [10.1007/s11214-005-5097-2](https://doi.org/10.1007/s11214-005-5097-2)

Cannizzo, J. K., Lee, H. M., & Goodman, J. 1990, ApJ, 351, 38, doi: [10.1086/168442](https://doi.org/10.1086/168442)

Cendes, Y., Berger, E., Alexander, K. D., et al. 2024, ApJ, 971, 185, doi: [10.3847/1538-4357/ad5541](https://doi.org/10.3847/1538-4357/ad5541)

Chambers, K. C., Magnier, E. A., Metcalfe, N., et al. 2016, arXiv e-prints, arXiv:1612.05560. <https://arxiv.org/abs/1612.05560>

Charalampopoulos, P., Leloudas, G., Malesani, D. B., et al. 2022, A&A, 659, A34, doi: [10.1051/0004-6361/202142122](https://doi.org/10.1051/0004-6361/202142122)

Davis, S. W., & El-Abd, S. 2019, ApJ, 874, 23, doi: [10.3847/1538-4357/ab05c5](https://doi.org/10.3847/1538-4357/ab05c5)

Davis, S. W., & Hubeny, I. 2006, ApJS, 164, 530, doi: [10.1086/503549](https://doi.org/10.1086/503549)

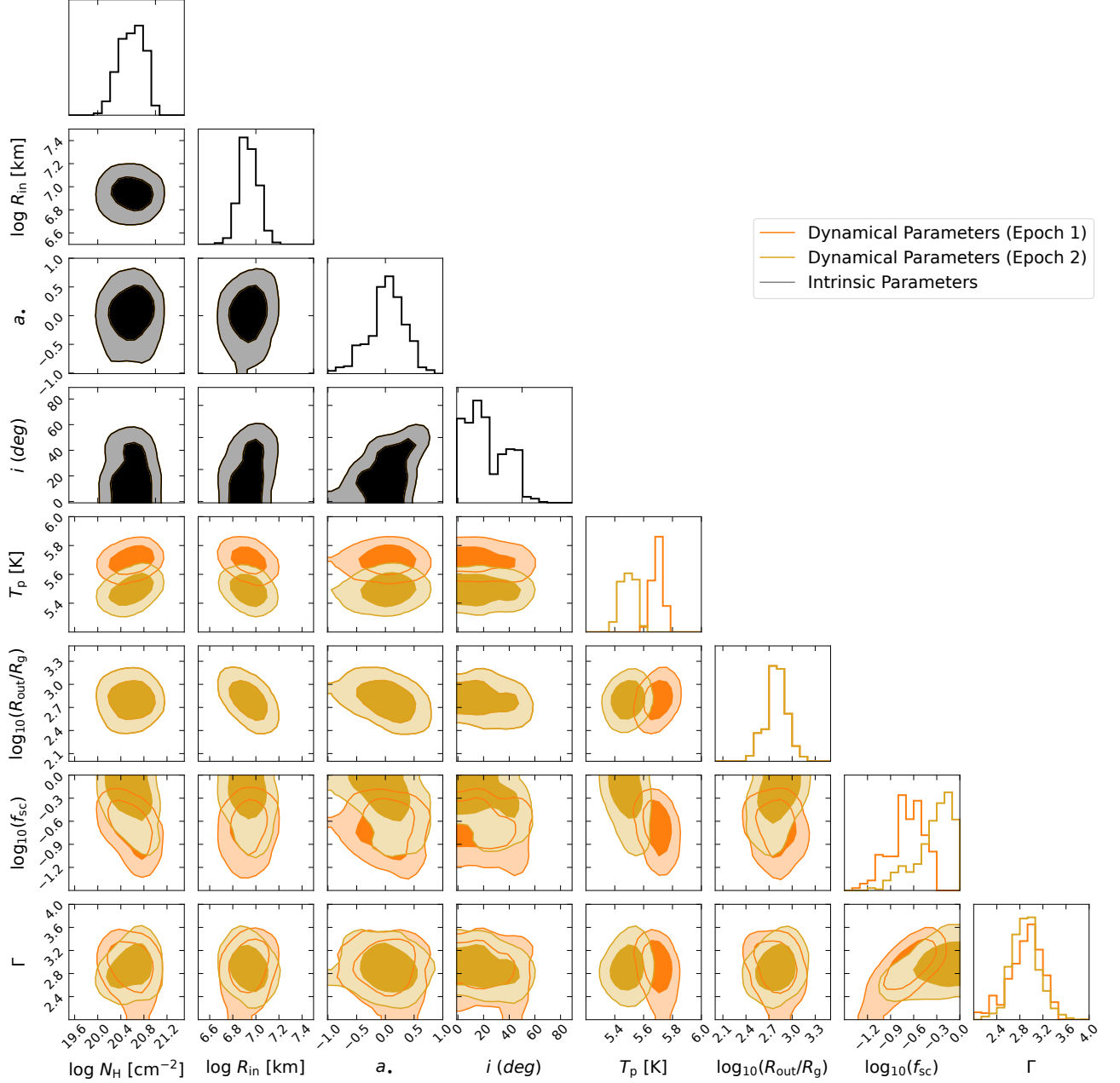


Figure 6. Full parameter posterior for the free parameters of our two epoch SED fitting. Intrinsic parameters are shown in black, while dynamical parameters are shown in orange and gold, respectively for the first and second epoch. Contour represent 68% and 95% credible interval of the projected two parameters.

Dosopoulou, F., & Antonini, F. 2017, ApJ, 840, 31,

doi: [10.3847/1538-4357/aa6b58](https://doi.org/10.3847/1538-4357/aa6b58)

Dvorkin, I., & Barausse, E. 2017, MNRAS, 470, 4547,

doi: [10.1093/mnras/stx1454](https://doi.org/10.1093/mnras/stx1454)

Evans, P. A., Beardmore, A. P., Page, K. L., et al. 2007,

A&A, 469, 379, doi: [10.1051/0004-6361:20077530](https://doi.org/10.1051/0004-6361:20077530)

Gabriel, C., Denby, M., Fyfe, D. J., et al. 2004, in Astronomical Society of the Pacific Conference Series, Vol. 314, Astronomical Data Analysis Software and Systems (ADASS) XIII, ed. F. Ochsenbein, M. G. Allen, & D. Egret, 759
 Gebhardt, K., Rich, R. M., & Ho, L. C. 2005, ApJ, 634, 1093, doi: [10.1086/497023](https://doi.org/10.1086/497023)
 Gehrels, N., Chincarini, G., Giommi, P., et al. 2004, ApJ, 611, 1005, doi: [10.1086/422091](https://doi.org/10.1086/422091)

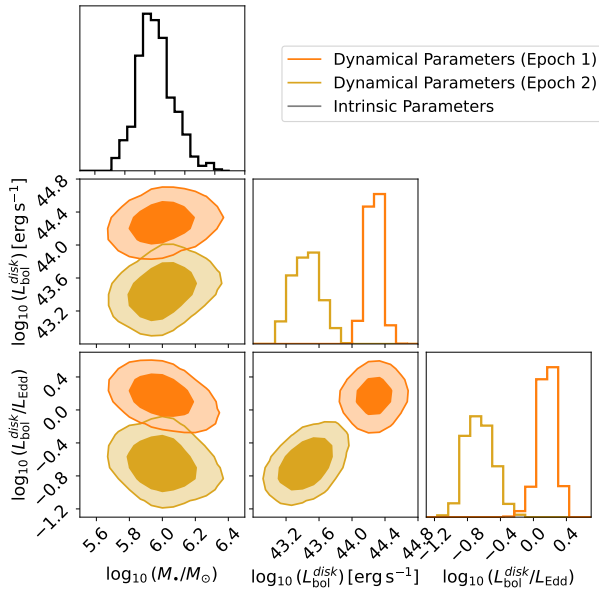


Figure 7. Full parameter posterior for secondary/derived parameters. Contours and labels as in Fig. 6.

Gezari, S., Heckman, T., Cenko, S. B., et al. 2009, ApJ, 698, 1367, doi: [10.1088/0004-637X/698/2/1367](https://doi.org/10.1088/0004-637X/698/2/1367)

Gezari, S., Hammerstein, E., Yao, Y., et al. 2021, Transient Name Server AstroNote, 103, 1

Governato, F., Colpi, M., & Maraschi, L. 1994, MNRAS, 271, 317, doi: [10.1093/mnras/271.2.317](https://doi.org/10.1093/mnras/271.2.317)

Greene, J. E., Strader, J., & Ho, L. C. 2020, ARA&A, 58, 257, doi: [10.1146/annurev-astro-032620-021835](https://doi.org/10.1146/annurev-astro-032620-021835)

Grotova, I., Rau, A., Baldini, P., et al. 2025, A&A, 697, A159, doi: [10.1051/0004-6361/202553669](https://doi.org/10.1051/0004-6361/202553669)

Gültekin, K., Richstone, D. O., Gebhardt, K., et al. 2009, ApJ, 698, 198, doi: [10.1088/0004-637X/698/1/198](https://doi.org/10.1088/0004-637X/698/1/198)

Guolo, M., Gezari, S., Yao, Y., et al. 2024, ApJ, 966, 160, doi: [10.3847/1538-4357/ad2f9f](https://doi.org/10.3847/1538-4357/ad2f9f)

Guolo, M., & Mummery, A. 2025, ApJ, 978, 167, doi: [10.3847/1538-4357/ad990a](https://doi.org/10.3847/1538-4357/ad990a)

Guolo, M., Mummery, A., Ingram, A., et al. 2025a, arXiv e-prints, arXiv:2504.20148, doi: [10.48550/arXiv.2504.20148](https://doi.org/10.48550/arXiv.2504.20148)

Guolo, M., Mummery, A., van Velzen, S., et al. 2025b, arXiv e-prints, arXiv:2510.26774, doi: [10.48550/arXiv.2510.26774](https://doi.org/10.48550/arXiv.2510.26774)

Haberle, M., Neumayer, N., Seth, A., et al. 2024, Nature, 631, 285, doi: [10.1038/s41586-024-07511-z](https://doi.org/10.1038/s41586-024-07511-z)

Hammerstein, E., van Velzen, S., Gezari, S., et al. 2022, arXiv e-prints, arXiv:2203.01461. <https://arxiv.org/abs/2203.01461>

—. 2023, ApJ, 942, 9, doi: [10.3847/1538-4357/aca283](https://doi.org/10.3847/1538-4357/aca283)

HI4PI Collaboration, Ben Bekhti, N., Flöer, L., et al. 2016, A&A, 594, A116, doi: [10.1051/0004-6361/201629178](https://doi.org/10.1051/0004-6361/201629178)

Hills, J. G. 1975, Nature, 254, 295, doi: [10.1038/254295a0](https://doi.org/10.1038/254295a0)

Hubeny, I., Blaes, O., Krolik, J. H., & Agol, E. 2001, ApJ, 559, 680, doi: [10.1086/322344](https://doi.org/10.1086/322344)

Inayoshi, K., Visbal, E., & Haiman, Z. 2020, ARA&A, 58, 27, doi: [10.1146/annurev-astro-120419-014455](https://doi.org/10.1146/annurev-astro-120419-014455)

Jin, C. C., Li, D. Y., Jiang, N., et al. 2025, arXiv e-prints, arXiv:2501.09580, doi: [10.48550/arXiv.2501.09580](https://doi.org/10.48550/arXiv.2501.09580)

Kormendy, J., & Ho, L. C. 2013, ARA&A, 51, 511, doi: [10.1146/annurev-astro-082708-101811](https://doi.org/10.1146/annurev-astro-082708-101811)

Lin, D., Strader, J., Carrasco, E. R., et al. 2018, Nature Astronomy, 2, 656, doi: [10.1038/s41550-018-0493-1](https://doi.org/10.1038/s41550-018-0493-1)

Lin, D., Strader, J., Romanowsky, A. J., et al. 2020, ApJL, 892, L25, doi: [10.3847/2041-8213/ab745b](https://doi.org/10.3847/2041-8213/ab745b)

Lynden-Bell, D., & Pringle, J. E. 1974, MNRAS, 168, 603, doi: [10.1093/mnras/168.3.603](https://doi.org/10.1093/mnras/168.3.603)

Magnier, E. A., Chambers, K. C., Flewelling, H. A., et al. 2020a, ApJS, 251, 3, doi: [10.3847/1538-4365/abb829](https://doi.org/10.3847/1538-4365/abb829)

Magnier, E. A., Sweeney, W. E., Chambers, K. C., et al. 2020b, ApJS, 251, 5, doi: [10.3847/1538-4365/abb82c](https://doi.org/10.3847/1538-4365/abb82c)

Masci, F. J., Laher, R. R., Rusholme, B., et al. 2019, PASP, 131, 018003, doi: [10.1088/1538-3873/aae8ac](https://doi.org/10.1088/1538-3873/aae8ac)

—. 2023, arXiv e-prints, arXiv:2305.16279, doi: [10.48550/arXiv.2305.16279](https://doi.org/10.48550/arXiv.2305.16279)

Mockler, B., Guillochon, J., & Ramirez-Ruiz, E. 2019, ApJ, 872, 151, doi: [10.3847/1538-4357/ab010f](https://doi.org/10.3847/1538-4357/ab010f)

Mummery, A. 2021, MNRAS, 507, L24, doi: [10.1093/mnrasl/slab088](https://doi.org/10.1093/mnrasl/slab088)

—. 2026, arXiv e-prints, arXiv:2601.14483, doi: [10.48550/arXiv.2601.14483](https://doi.org/10.48550/arXiv.2601.14483)

Mummery, A., & Balbus, S. A. 2020, MNRAS, 492, 5655, doi: [10.1093/mnras/staa192](https://doi.org/10.1093/mnras/staa192)

Mummery, A., Metzger, B., van Velzen, S., & Guolo, M. 2025, arXiv e-prints, arXiv:2512.09143, doi: [10.48550/arXiv.2512.09143](https://doi.org/10.48550/arXiv.2512.09143)

Mummery, A., Nathan, E., Ingram, A., & Gardner, M. 2024a, arXiv e-prints, arXiv:2408.15048, doi: [10.48550/arXiv.2408.15048](https://doi.org/10.48550/arXiv.2408.15048)

Mummery, A., & van Velzen, S. 2025, arXiv e-prints, arXiv:2410.17087, doi: [10.48550/arXiv.2410.17087](https://doi.org/10.48550/arXiv.2410.17087)

Mummery, A., van Velzen, S., Nathan, E., et al. 2024b, MNRAS, 527, 2452, doi: [10.1093/mnras/stad3001](https://doi.org/10.1093/mnras/stad3001)

Mummery, A., Wevers, T., Saxton, R., & Pasham, D. 2023, MNRAS, 519, 5828, doi: [10.1093/mnras/stac3798](https://doi.org/10.1093/mnras/stac3798)

Patra, K. C., Foley, R. J., Earl, N., et al. 2025, arXiv e-prints, arXiv:2510.12572, doi: [10.48550/arXiv.2510.12572](https://doi.org/10.48550/arXiv.2510.12572)

Pechetti, R., Seth, A., Kamann, S., et al. 2022, ApJ, 924, 48, doi: [10.3847/1538-4357/ac339f](https://doi.org/10.3847/1538-4357/ac339f)

Pfeffer, J., Griffen, B. F., Baumgardt, H., & Hilker, M. 2014, MNRAS, 444, 3670, doi: [10.1093/mnras/stu1705](https://doi.org/10.1093/mnras/stu1705)

Ramsden, P., Lanning, D., Nicholl, M., & McGee, S. L. 2022, MNRAS, 515, 1146, doi: [10.1093/mnras/stac1810](https://doi.org/10.1093/mnras/stac1810)

Ramsden, P., Nicholl, M., McGee, S. L., & Mummary, A. 2025, MNRAS, 541, 1218, doi: [10.1093/mnras/staf1059](https://doi.org/10.1093/mnras/staf1059)

Rees, M. J. 1988, Nature, 333, 523, doi: [10.1038/333523a0](https://doi.org/10.1038/333523a0)

Reines, A. E., & Volonteri, M. 2015, ApJ, 813, 82, doi: [10.1088/0004-637X/813/2/82](https://doi.org/10.1088/0004-637X/813/2/82)

Reynolds, T. M., Thomsen, L., Mattila, S., et al. 2025, arXiv e-prints, arXiv:2506.18489, doi: [10.48550/arXiv.2506.18489](https://doi.org/10.48550/arXiv.2506.18489)

Ricarte, A., & Natarajan, P. 2018, MNRAS, 481, 3278, doi: [10.1093/mnras/sty2448](https://doi.org/10.1093/mnras/sty2448)

Ricarte, A., Tremmel, M., Natarajan, P., & Quinn, T. 2021a, ApJL, 916, L18, doi: [10.3847/2041-8213/ac1170](https://doi.org/10.3847/2041-8213/ac1170)

Ricarte, A., Tremmel, M., Natarajan, P., Zimmer, C., & Quinn, T. 2021b, MNRAS, 503, 6098, doi: [10.1093/mnras/stab866](https://doi.org/10.1093/mnras/stab866)

Roming, P. W. A., Kennedy, T. E., Mason, K. O., et al. 2005, SSRv, 120, 95, doi: [10.1007/s11214-005-5095-4](https://doi.org/10.1007/s11214-005-5095-4)

Roth, N., Rossi, E. M., Krolik, J., et al. 2020, SSRv, 216, 114, doi: [10.1007/s11214-020-00735-1](https://doi.org/10.1007/s11214-020-00735-1)

Schlafly, E. F., & Finkbeiner, D. P. 2011, ApJ, 737, 103, doi: [10.1088/0004-637X/737/2/103](https://doi.org/10.1088/0004-637X/737/2/103)

Seth, A. C., van den Bosch, R., Mieske, S., et al. 2014, Nature, 513, 398, doi: [10.1038/nature13762](https://doi.org/10.1038/nature13762)

Shakura, N. I., & Sunyaev, R. A. 1973, A&A, 24, 337

Shimura, T., & Takahara, F. 1995, ApJ, 445, 780, doi: [10.1086/175740](https://doi.org/10.1086/175740)

Steiner, J. F., Narayan, R., McClintock, J. E., & Ebisawa, K. 2009, PASP, 121, 1279, doi: [10.1086/648535](https://doi.org/10.1086/648535)

Strüder, L., Briel, U., Dennerl, K., et al. 2001, A&A, 365, L18, doi: [10.1051/0004-6361:20000066](https://doi.org/10.1051/0004-6361:20000066)

Taylor, M. A., Tahmasebzadeh, B., Thompson, S., et al. 2025, ApJL, 991, L24, doi: [10.3847/2041-8213/ae028e](https://doi.org/10.3847/2041-8213/ae028e)

Tremmel, M., Governato, F., Volonteri, M., Pontzen, A., & Quinn, T. R. 2018a, ApJL, 857, L22, doi: [10.3847/2041-8213/aabc0a](https://doi.org/10.3847/2041-8213/aabc0a)

Tremmel, M., Governato, F., Volonteri, M., & Quinn, T. R. 2015, MNRAS, 451, 1868, doi: [10.1093/mnras/stv1060](https://doi.org/10.1093/mnras/stv1060)

Tremmel, M., Governato, F., Volonteri, M., Quinn, T. R., & Pontzen, A. 2018b, MNRAS, 475, 4967, doi: [10.1093/mnras/sty139](https://doi.org/10.1093/mnras/sty139)

van Velzen, S., Farrar, G. R., Gezari, S., et al. 2011, ApJ, 741, 73, doi: [10.1088/0004-637X/741/2/73](https://doi.org/10.1088/0004-637X/741/2/73)

van Velzen, S., Gezari, S., Hammerstein, E., et al. 2021, ApJ, 908, 4, doi: [10.3847/1538-4357/abc258](https://doi.org/10.3847/1538-4357/abc258)

Van Wassenhove, S., Capelo, P. R., Volonteri, M., et al. 2014, MNRAS, 439, 474, doi: [10.1093/mnras/stu024](https://doi.org/10.1093/mnras/stu024)

Voggel, K. T., Seth, A. C., Baumgardt, H., et al. 2019, ApJ, 871, 159, doi: [10.3847/1538-4357/aaf735](https://doi.org/10.3847/1538-4357/aaf735)

Volonteri, M., Lodato, G., & Natarajan, P. 2008, MNRAS, 383, 1079, doi: [10.1111/j.1365-2966.2007.12589.x](https://doi.org/10.1111/j.1365-2966.2007.12589.x)

Volonteri, M., & Perna, R. 2005, MNRAS, 358, 913, doi: [10.1111/j.1365-2966.2005.08832.x](https://doi.org/10.1111/j.1365-2966.2005.08832.x)

Waters, C. Z., Magnier, E. A., Price, P. A., et al. 2020, ApJS, 251, 4, doi: [10.3847/1538-4365/abb82b](https://doi.org/10.3847/1538-4365/abb82b)

Yao, Y., Ravi, V., Gezari, S., et al. 2023, ApJL, 955, L6, doi: [10.3847/2041-8213/acf216](https://doi.org/10.3847/2041-8213/acf216)

Yao, Y., Chornock, R., Ward, C., et al. 2025, ApJL, 985, L48, doi: [10.3847/2041-8213/add7de](https://doi.org/10.3847/2041-8213/add7de)

Yuan, W., Zhang, C., Ling, Z., et al. 2018, in Society of Photo-Optical Instrumentation Engineers (SPIE) Conference Series, Vol. 10699, Space Telescopes and Instrumentation 2018: Ultraviolet to Gamma Ray, ed. J.-W. A. den Herder, S. Nikzad, & K. Nakazawa, 1069925, doi: [10.1117/12.2313358](https://doi.org/10.1117/12.2313358)